Received: 11 March 2021 | Revised: 1 June 2021 | Accepted: 4 June 2021 | Published online: 24 July 2021

DOI: 10.1002/dad2.12218

Alzheimer's & Dementia
Diagnosis, Assessment & Disease Monitoring

RESEARCH ARTICLE

Hippocampal subfield imaging and fractional anisotropy show parallel changes in Alzheimer's disease tau progression using simultaneous tau-PET/MRI at 3T

Mackenzie L. Carlson[1] | **Tyler N. Toueg**[2] | **M. Mehdi Khalighi**[3] | **Jessa Castillo**[3] | **Bin Shen**[3] | **Emily C. Azevedo**[3] | **Phillip DiGiacomo**[1] | **Nicole Mouchawar**[3] | **Gustavo Chau**[1] | **Greg Zaharchuk**[3] | **Michelle L. James**[2,3] | **Elizabeth C. Mormino**[2] | **Michael M. Zeineh**[3]

[1] Department of Bioengineering, Stanford University, Stanford, California, USA

[2] Department of Neurology, Stanford University, Stanford, California, USA

[3] Department of Radiology, Stanford University, Stanford, California, USA

Correspondence
Michael M. Zeineh, Clinical Neuroradiology, 300 Pasteur Dr, MC 5105, Stanford, CA 94305, USA.
E-mail: mzeineh@stanford.edu

Funding information
National Science Foundation, Grant/Award Number: DGE-1656518; NIA, Grant/Award Numbers: R01AG061120, R01 AG048076, K01 AG051718, R21 AG058859; Alzheimer's Disease and Neurocognitive Disorders; Doris Duke Charitable Foundation; Stanford Wu Tsai Neuroscience Institute; Stanford Precision Health and Integrated Diagnostics Center

Abstract

Introduction: Alzheimer's disease (AD) is the most common form of dementia, characterized primarily by abnormal aggregation of two proteins, tau and amyloid beta. We assessed tau pathology and white matter connectivity changes in subfields of the hippocampus simultaneously in vivo in AD.

Methods: Twenty-four subjects were scanned using simultaneous time-of-flight ^{18}F-PI-2620 tau positron emission tomography/3-Tesla magnetic resonance imaging and automated segmentation.

Results: We observed extensive tau elevation in the entorhinal/perirhinal regions, intermediate tau elevation in cornu ammonis 1/subiculum, and an absence of tau elevation in the dentate gyrus, relative to controls. Diffusion tensor imaging showed parahippocampal gyral fractional anisotropy was lower in AD and mild cognitive impairment compared to controls and strongly correlated with early tau accumulation in the entorhinal and perirhinal cortices.

Discussion: This study demonstrates the potential for quantifiable patterns of ^{18}F-PI2620 binding in hippocampus subfields, accompanied by diffusion and volume metrics, to be valuable markers of AD.

KEYWORDS
^{18}F-PI-2620, Alzheimer's disease, diffusion, hippocampus, magnetic resonance imaging

HIGHLIGHTS

- Tau standardized uptake value ration (SUVr) corresponded with known pathological progression of tau accumulation.
- Entorhinal and perirhinal cortices (ERC/PRC) tau SUVr correlates with parahippocampal gyral fractional anisotropy, especially for amnestic subjects.
- Tau deposition is more strongly correlated to volume loss in ERC/PRC than in whole hippocampus.

RESEARCH IN CONTEXT

1. **Systematic review**: The authors reviewed literature using PubMed and Google Scholar sources. Few studies have focused on detecting subtle differences in tau progression and white matter integrity on the spatial scale of hippocampal subfields, though relevant references on hippocampal subfields or Alzheimer's disease (AD) biomarkers are cited as appropriate.
2. **Interpretation**: Our positron emission tomography/magnetic resonance imaging (PET/MRI) results are consistent with ex vivo and neuropathological work showing that tau corresponds to cognitive decline and is thought to be associated more closely with neurodegeneration and a loss of white matter connectivity than amyloid beta. These findings also build off previous imaging work on the whole hippocampal scale.
3. **Future directions**: These findings underline the potential for using PET/MRI to track AD pathology in vivo, which could help with earlier diagnosis, patient stratification, and treatment monitoring.

1 | INTRODUCTION

Alzheimer's disease (AD) is a progressive neurological disorder resulting in severe cognitive and behavioral deficits affecting nearly 6 million adults in the United States alone.[1] Two main pathologic features of AD are the aggregation of extracellular amyloid beta (Aβ) and intracellular hyperphosphorylated tau. Cross-sectional neuropathological studies have determined that tau has a characteristic pattern of accumulation in the brain throughout the progression of amnestic AD. Accumulation begins in the transentorhinal region, progresses to the entorhinal region, then the hippocampal formation (including subiculum, cornu ammonis fields [CA1-3], and dentate gyrus) while simultaneously spreading to the adjacent neocortex and beyond.[2] Studies have shown that connectivity and white matter integrity may be more closely associated with tau than Aβ deposition,[3,4] and tau aggregation correlates with severity of cognitive deficits and synaptic and neuronal loss.[5]

Mounting evidence shows that the hippocampus is particularly atrophied during amnestic AD, but that functionally and cytoarchitecturally distinct subregions of the hippocampus may have differential sensitivity.[6–8] Tau in the entorhinal region may instigate volume loss, weakened connectivity, and metabolic reduction in spatially and functionally adjacent brain areas due to microtubule instability, which contributes to axonal degeneration and reduced synaptic transmission.[9,10] Ex vivo work has shown a characteristic progression of tau in AD and has allowed scientists to study tau seeding and AD onset.[2,11] However, in vivo work, especially including non-invasive magnetic resonance imaging (MRI) and positron emission tomography (PET) imaging, is critical for studying hippocampal subfield pathology throughout disease progression in living humans. Such studies could ultimately aid in earlier diagnosis and future tracking and treatment in human patients. In vivo imaging studies have begun exploring region-specific pathologically induced changes using PET and MRI, but few have been able to demonstrate disease-related pathologic progression on the spatial scale of hippocampal subfields. Prior tau-PET imaging studies have shown that patterns of tracer uptake in the whole brain correspond to neuropathological staging, but this work has been limited to whole-hippocampal analysis due to resolution limits of PET imaging.[12,13] Here, we use time-of-flight (TOF) imaging capability, 2D erosion for minimizing partial volume effects, and a custom hippocampal atlas to enable subfield segmentation of PET images.[14]

Diffusion tensor imaging (DTI) MRI has also been used to study connectivity and white matter degradation in the brain, complementary to structural MRI volume reductions in AD.[15,16] DTI is important to study in the context of AD to evaluate white matter connectivity within functionally connected regions of the medial temporal lobe.[17] Lower connectivity has been associated with reduced memory performance in amnestic AD and MCI subjects.[18]

Our prior work has used simultaneous PET-MR and hippocampal segmentation techniques to analyze subfield-specific measures of volume and glucose metabolism.[14] However, few studies have investigated tau uptake in vivo on a hippocampal subfield-specific level in concert with volumetric and microstructural measurements which—given the characteristic progression of tau with disease severity—is important for the study of onset and real-time progression of AD. We use a tracer with low choroid plexus binding, ^{18}F-PI-2620, which, in contradistinction to other tracers, does not obscure hippocampal uptake.[19,20] Thus, we aim to simultaneously analyze tau-PET uptake, volume, and connectivity of related subregions within and surrounding the hippocampus. By studying hippocampal subfield-specific differences in tau burden, white matter degradation, and volume, we may be able to better understand the relationship between the patterns of several disease-specific changes in vivo, which could ultimately lead to earlier diagnosis and future treatments for AD.

Here, we show that using simultaneous tau-PET/MRI and fine-tuned registration, we can detect subtle differences in tau tracer accumulation and volume within hippocampal subfields that is consistent with

TABLE 1 Subject demographics

	AD	MCI	Control
Age	68.8 ± 10.64 years	71.2 ± 8.47 years	71.5 ± 8.75 years
N	5	6	13
Sex (M/F)	2/3	2/4	10/3
Amnestic	3	5	N/A

Abbreviations: AD, Alzheimer's disease; MCI, mild cognitive impairment.

known histological patterning. We also show, using both region of interest (ROI)- and tractographic-based DTI, that subfield tau burden correlates with white matter degradation in the parahippocampal gyrus.

2 | METHODS

2.1 | Subjects

A total of 24 subjects (Table 1, five amyloid-positive probable AD, six amyloid-positive mild cognitive impairment [MCI], and 13 healthy control subjects) classified by clinical consensus of neurologists and neuropsychologists at Stanford University were included. Amyloid status is not known for controls. In accordance with the Stanford University Institutional Review Board (IRB) and the Health Insurance Portability and Accountability Act, healthy controls were enrolled from the Stanford Aging and Memory Study,[21] and patients were enrolled from either the Alzheimer's Disease Research Center (ADRC) or the Stanford Center for Memory Disorders.[19] Written informed consent was obtained from all participants or their legally authorized representative under protocols approved by the IRB at Stanford. All AD and MCI subjects were confirmed to have biomarker evidence of amyloid positivity using cerebrospinal fluid or amyloid PET scans.

2.2 | Image acquisition

Subjects underwent a dynamic 90-minute tau-PET scan on a 3T PET-MR (SIGNA, GE) using time-of-flight (TOF) capability after a 5-10mCi intravenous injection of ^{18}F-PI-2620 (Life Molecular Imaging, Inc.). During the PET acquisition, we acquired a sagittal T1-weighted inversion recovery spoiled gradient echo (IRFSPGR; TR 7.6 ms, TE 3.1 ms, FA 11, 1 × 1 × 1.2 mm resolution, 5m46s scan time) and a coronal-oblique T2-weighted fast spin echo (FSE; TR 14111 ms, TE 102.4 ms, FA 111, 0.43 × 0.43 × 1.9 mm resolution, 3m24s scan time). A subset of subjects (N = 21, five amyloid-positive AD [three amnestic], five amyloid-positive MCI [four amnestic], and 11 healthy controls) had DTI acquired (6 b = 0 s/mm^2, 30 to 60 b = 1000s/mm^2 directions, 1.6 to 2.0 mm isotropic, and an additional 3 to 6 blip-down b = 0 s/mm^2 image).[22] Note, voxel size was included as a covariate in initial analyses, which did not change the significance of any results. A LAVA-Flex (liver-accelerated volume acquisition-Flex) MRI series was used, along with an atlas-based segmentation algorithm, to classify fat, water, air, and bone in the head and construct subject-specific attenuation correction maps for PET reconstruction.[22]

2.3 | PET image processing

Standardized uptake value (SUV) maps were reconstructed from static images by summing the 30-minute interval between 60 and 90 minutes of dynamic PET data using TOF optimized subset expectation maximization (TOF-OSEM) with three iterations, 28 subsets, 2.78 × 1.17 × 1.17 mm voxel size, and zero-TE MR attenuation correction. SUV maps were normalized to the inferior cerebellar cortex (to account for any off-target binding effects[23]) of each subject using a modified FreeSurfer segmentation to produce SUV ratio (SUVr) maps. SUVr maps were precisely registered to coronal T2 MR image space using the T1-weighted IRFSPGR as an intermediate registration volume using niftireg.[24] Coronal T2 space was used for analysis to preserve accuracy of hippocampal subfield segmentations.

2.4 | Subfield segmentation

Hippocampal subfields were segmented using Automated Segmentation of Hippocampal Subfields (ASHS, Penn Image Computing & Science Lab), which combines multi-atlas label fusion and machine learning for error correction to precisely segment hippocampal substructures, using a custom atlas.[25,26] Segmentations were verified manually for accuracy. Analyzed subfields were: cornu ammonis 1 (CA1), dentate gyrus and CA2-4 as one combined subfield (DG), subiculum (SUB), entorhinal and perirhinal cortices (ERC/PRC), and white matter within the parahippocampal gyrus (PHG). Due to the small size of subfields CA2-4 and the dentate gyrus, these regions are commonly grouped together.[27] The fornix was included from a FreeSurfer 6.0 segmentation. Hippocampal subfield volumes were calculated in coronal T2 MR space, and DTI and PET images were mapped into the same space to quantify mean fractional anisotropy (FA) and mean diffusivity (MD), and SUVr (respectively). Subfields were eroded by one voxel in the 2D oblique coronal plane, using the command c3d with the "-erode" flag and 1 × 1 × 0 option, to reduce partial volume effects in PET imaging.[28] SUV was computed by taking the average SUV across CA1, DG, SUB, and ERC/PRC. FA/MD was similarly computed across the subfields and PHG. We have previously validated these methods with analysis of FDG-PET and volume measures across hippocampal subfields in a separate AD cohort[14] (Figure 1).

2.5 | DTI image processing

Diffusion images were pre-processed with FDT (FMRIB's Diffusion Toolbox) using top-up susceptibility-induced distortion correction, brain extraction, and eddy distortion correction.[29,30]

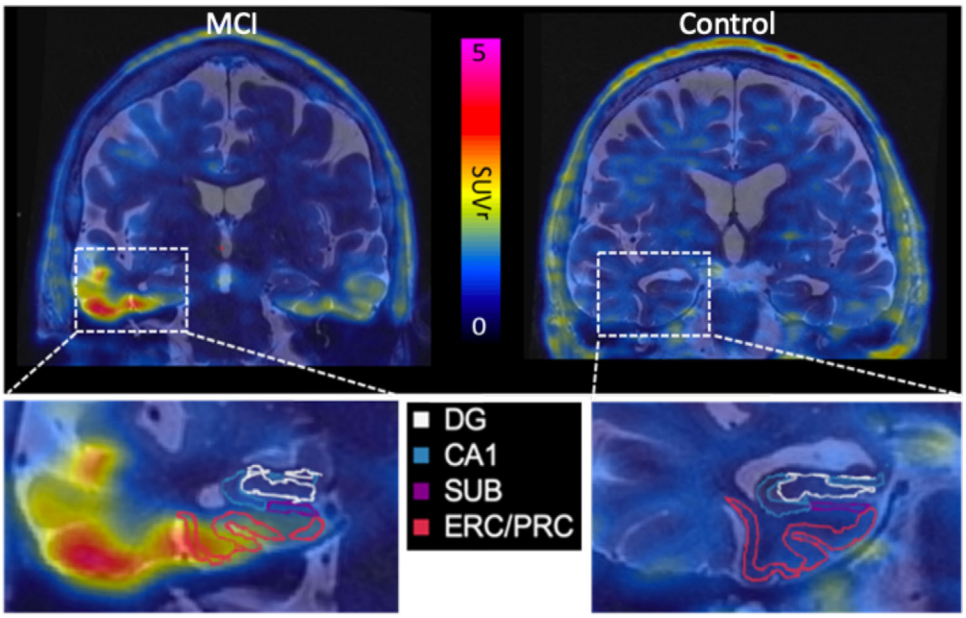

FIGURE 1 Tau-positron emission tomography (PET) standardized uptake value (SUV) mapped on to coronal T2 magnetic resonance (MR) image with hippocampal subfields outlined on a mild cognitive impairment (MCI; left) and control subject (right). DG, dentate gyrus; CA1, cornu ammonis 1; ERC/PRC, entorhinal and perirhinal cortices; SUB, subiculum

Weighted-least-squares tensor fitting using DTIFIT generated FA and mean diffusivity MDmaps,[31] which indicate the degree of asymmetry of water diffusion directionality (which is sensitive to microstructural changes) and measure overall diffusion (which is increased with decreased cellularity/cellular processes), respectively. Diffusion images were also fitted to the neurite orientation dispersion and density imaging (NODDI) algorithm to generate free water volume fraction (FISO) and orientation dispersion index (ODI) maps.[32] FICVF was not computed as we had only one non-zero b shell. The b = 0s/mm^2 images for each subject were registered to coronal-oblique T2-weighted images using reg_aladin,[24] then FA, MD, FISO, and ODI images were resampled to coronal oblique T2-weighted image space using the b = 0-to-T2 image transformation matrix.

We then performed a tract-based analysis: tractography was computed using bedpostx in FMRIB's diffusion toolbox, which implements a probabilistic multi-fiber ball-and-stick diffusion model, followed by probtrackx.[33] The –opd, –l, and –f flags, which, respectively, output path distribution maps, perform loop checks on paths, and use anisotropy to constrain tracking, were used. The choice of flags used was based on comparing Dice coefficients between this and other methods; the result showed least overlap among distinct tracts. Target/seed pairs included the following tracts (1) parahippocampal cingulum: anterior to/from posterior parahippocampal gyrus, (2) perforant pathway: ERC/PRC to/from DG/CA4/3 and CA1, (3) Schaffer collaterals: DG/CA4/3 to/from CA1, (4) CA1 to/from SUB, and finally (5) SUB to/from ERC/PRC. The corpus collosum was used as an exclusion mask. The combined bidirectional tracts were normalized to total track number to show probability maps of streamline counts, and probability-weighted average DTI metrics (FA, MD, ODI, and FISO) were computed. Bilateral DTI results were combined using a volume-weighted average.

2.6 | Statistical analysis

Volume: Separate linear regression analyses were completed on bilateral whole hippocampus (all subfields combined) and individual bilateral subfield (CA1, DG, SUB, ERC/PRC, PHG) volume. Volume regressions used volume as the dependent variable and disease status as the independent variable, with total intracranial volume (estimated by FreeSurfer 6.0[34]) and age as additional independent regressors. We reported the uncorrected *P*-value for the disease status regressor and computed an associated Cohen's D score. AD (n = 5) and MCI (n = 6) subjects were combined to better balance the groups and compared to controls (n = 13). Analyses were also repeated using combined amnestic AD (n = 3) and MCI (n = 5) subjects. Finally, we compared all AD to all MCI, and all MCI to controls using the same model.

PET: Separate linear regression analyses were performed for tau SUVr using the same whole hippocampus and subfield combinations. SUVr was the dependent variable and disease status was the independent variable, with age as an independent regressor. We similarly combined AD (n = 5) and MCI (n = 6), separately analyzed combined amnestic AD (n = 3) and MCI (n = 5) subjects, and compared all AD to all MCI and all MCI to controls (n = 13). Pearson correlation analyses were performed between raw volume and raw SUVr measurements within each subfield.

DTI: Separate linear regression analyses were performed for each DTI metric (FA, MD, ODI, and FISO) using the same whole hippocampus and subfield combinations, with the addition of the PHG, fornix, and tract-based DTI metrics. The DTI metric was the dependent variable and disease status was the independent variable, with age as an independent regressor. We similarly combined AD (n = 5) and MCI (n = 5). For regions that showed a significant difference between AD/MCI

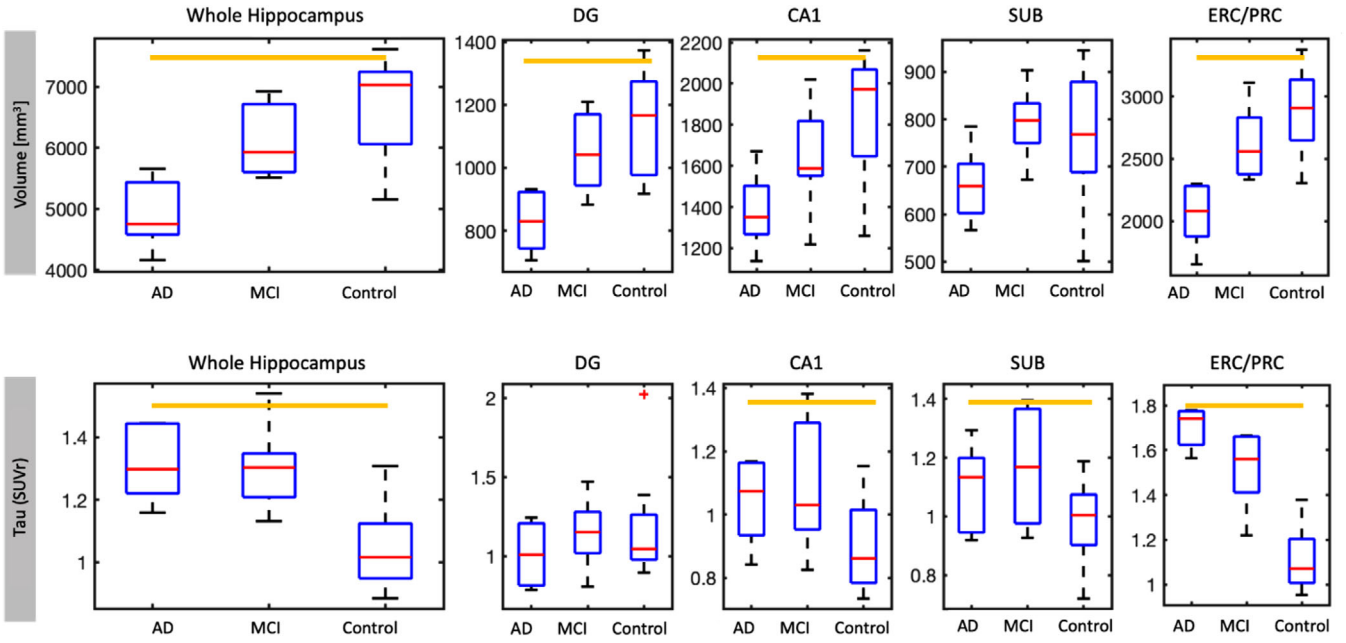

FIGURE 2 Boxplots showing volume (top) and standardized uptake value ratio (SUVr; bottom) in whole hippocampus and subfields across groups, including amnestic and non-amnestic subjects. Significance did not change when non-amnestic subjects were excluded. Volume datapoints have been adjusted for estimated total intracranial volume using residuals from a linear regression model centered about the mean volume. Orange bars indicate a significant difference between controls and the combined Alzheimer's disease (AD)/mild cognitive impairment (MCI) cohort. Note the scale bars are optimized for each subregion's dynamic range, DG, dentate gyrus; CA1, cornu ammonis 1; ERC/PRC, entorhinal and perirhinal cortices; SUB, subiculum

and controls (n = 11), we performed Pearson correlations between DTI metrics and tau SUVr in the ERC/PRC. Pearson correlation analyses were performed between diffusion tract-based measurements and SUVr within each corresponding connected subfield. For simplicity, results are organized by region.

Multiple comparison correction was performed using Li and Ji's method[35] to account for both covariance and independence between subregions, using the eigenvalues of the subfield covariance matrix to compute an effective number of degrees of freedom for each metric, and providing a *P*-value significance threshold for each test. All reported significant statistics are below this threshold unless otherwise specified. Regression residuals for all analyses performed showed normalcy. All statistical analyses were completed using STATA v15.0.

3 | RESULTS

3.1 | Volume

The combined AD/MCI group had smaller whole hippocampal volume compared to controls ($P = .002$). All subfields except SUB had significantly smaller volume in AD/MCI than controls (Figure 2, Table 2). When non-amnestic MCI and AD subjects were excluded, volume differences between AD/MCI and controls were significant in ERC/PRC ($P = .004$) and whole hippocampus ($P = .009$). Volume differences between AD and MCI subjects was significant in ERC/PRC ($P = .015$) and whole hippocampus ($P = .025$) and trending in DG ($P = .048$; Li and Ji threshold was $P < .025$). Volumes were not significantly different between MCI and controls for any subfield or whole hippocampus.

3.2 | Tau SUVr

Whole hippocampus SUVr was higher in AD/MCI than controls (Figure 2, Table 2, $P < .001$). Examining the subfields, SUVr was significantly higher in AD/MCI than controls in the ERC/PRC ($P < .001$), and to a lesser degree in CA1 ($P = .012$) and SUB ($P = .010$), but not DG ($P = .708$). The effect size of SUVr difference in ERC/PRC (D = −3.407) was larger than for whole hippocampus (D = −2.188). When non-amnestic subjects were excluded, SUVr differences between AD/MCI and controls were significant in CA1 ($P = .001$), SUB ($P = .001$), ERC/PRC ($P < .001$), and whole hippocampus ($P < .001$) but not DG ($P = .708$). There was a trend toward higher SUVr in AD compared to MCI in ERC/PRC only ($P = .017$). SUVr differences between MCI and controls were significant in ERC/PRC ($P < .001$), SUB ($P = .015$), and whole hippocampus ($P < .001$), and trending in CA1 ($P = .025$; Li and Ji threshold was $P < .017$). Correlations between tau SUVr and volume were highly significant in ERC/PRC ($R = -0.67$, $P < .001$), a trend in the whole hippocampus ($R = -0.42$, $P = .040$), and not significant in other subfields.

TABLE 2 Mean and standard deviation of volume and tau uptake SUVr in subfields, and results of linear regression statistics

	Volume [mm^3]	Volume *P*-value	Cohen's d	SUVr	SUVr *P*-value	Cohen's d	Correlation between volume, SUVr
Whole HC	AD/MCI: 5273 ± 898.3 Control: 6890 ± 790.8	**.002**	1.546	AD/MCI: 1.31 ± 0.131 Control: 1.05 ± 0.134	**<.001**	-2.188	**R = -0.423 P = .040**
DG	AD/MCI: 903 ± 157.9 Control: 1185 ± 201.7	**.010**	0.095	AD/MCI: 1.09 ± 0.221 Control: 1.15 ± 0.309	.708	0.151	R = 0.049P = .820
CA1	AD/MCI: 1432 ± 309.6 Control: 1917 ± 270.5	**.005**	1.322	AD/MCI: 1.07 ± 0.177 Control: 0.91 ± 0.135	**.012**	-1.121	R = -0.291P = 0.168
SUB	AD/MCI: 700 ± 120.6 Control: 794 ± 151.9	.528	0.271	AD/MCI: 1.13 ± 0.173 Control: 0.98 ± 0.135	**.010**	-1.148	R = -0.069P = 0.749
ERC/PRC	AD/MCI: 2238 ± 410.7 Control: 2293 ± 319.9	**.001**	1.721	AD/MCI: 1.60 ± 0.170 Control: 1.11 ± 0.124	**<.001**	-3.407	**R = -0.671 *P* < .001**

Note: Multiple comparison significance threshold for volume/SUVr was *P* = .025/.017.
Abbreviations: AD, Alzheimer's disease; CA1, cornu ammonis 1; DG, dentate gyrus; ERC/PRC, entorhinal and perirhinal cortices; MCI, mild cognitive impairment; SUB, subiculum; SUVr, standardized uptake value ratio.

TABLE 3 Parahippocampal gyral ROI and probability-weighted parahippocampal cingulum tract-based diffusion *P* comparing controls to AD/MCI

	FA	*P*	MD [e^{-4}]	*P*	ODI	*P*	FISO	*P*
PHG ROI	AD/MCI: 0.423 ± 0.0286 Control: 0.465 ± 0.0276	**.003**	AD/MCI: 7.02 ± 0.600 Control: 6.98 ± 0.300	.813	AD/MCI: 0.282 ± 0.0244 Control: 0.260 ± 0.0236	.044	AD/MCI: 0.0801 ± 0.02256 Control: 0.0740 ± 0.01267	.459
Parahippocamp cingulum	AD/MCI: 0.392 ± 0.0288 Control: 0.444 ± 0.0262	**.001**	AD/MCI: 7.14 ± 0.497 Control: 6.95 ± 0.292	.383	AD/MCI: 0.301 ± 0.0129 Control: 0.273 ± 0.0202	**.003**	AD/MCI: 0.0831 ± 0.01840 Control: 0.0718 ± 0.00985	.123

Abbreviations: AD, Alzheimer's disease; FA, functional anisotropy; FISO, free water volume fraction; MCI, mild cognitive impairment; MD, mean diffusivity; ODI, orientation dispersion index; PHG; parahippocampal gyrus; ROI, region of interest.

3.3 | DTI

In the PHG, FA is significantly lower in AD/MCI compared to controls (*P* = .003 for all AD/MCI, *P* = .004 for amnestic AD/MCI; Table 3, Table S1 in supporting information). ODI trended toward increasing in AD/MCI PHG (*P* = .044), while MD and FISO were not statistically different. Tractographic-based metrics showed comparatively more significant changes with lower FA (*P* = .001, T = –4.15) and higher ODI (*P* = .003, T = 3.47) in the anterior-posterior parahippocampal gyral cingulum bilaterally in AD/MCI subjects compared to controls (Table 3, Table S2 in supporting information). FA in the PHG negatively correlates (R = –0.60, *P* = .008) with ERC/PRC tau SUVr in amnestic AD/MCI and controls (Figure 3A-C), and this correlation holds (R = –0.53, *P* = .014) in all (amnestic and non-amnestic) AD/MCI and controls. Evaluation of parahippocampal gyral cingulum tractography metrics showed a significant negative correlation between FA and ERC/PRC SUVr (*P* = .008, R = –0.61) and a positive correlation between ODI and ERC/PRC SUVr (*P* = .009, R = 0.67).

In CA1, amnestic AD/MCI had significantly higher MD than controls (*P* = .008), although significance was reduced when all AD/MCI was included (*P* = .044). CA1 ODI trended toward being lower in all AD/MCI (*P* = .051). CA1 MD positively correlated with ERC/PRC SUVr in amnestic subjects (R = 0.49, *P* = .041). Correlation of tractographic-based metrics with tau SUVR revealed a positive correlation of CA1-

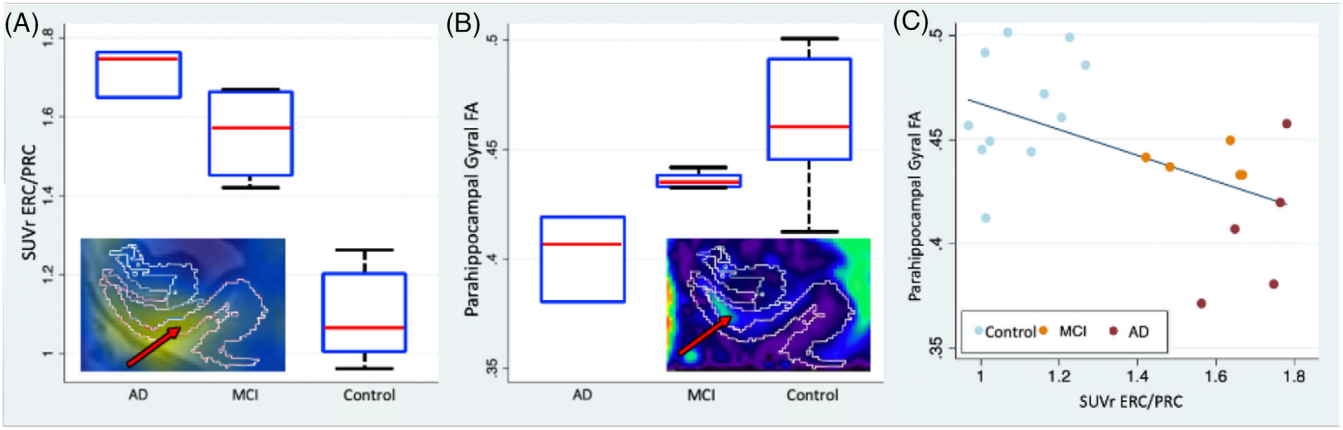

FIGURE 3 Boxplot of (A) tau standardized uptake value ratio (SUVr) in the entorhinal and perirhinal cortices (ERC/PRC) and (B) fractional anisotropy (FA) in the parahippocampal gyrus for amnestic Alzheimer's disease (AD), amnestic mild cognitive impairment (MCI), and controls. Hippocampal subfield diagrams in plot corners show segmentations overlaid on T2-w fused with (A) SUVr with ERC/PRC outlined in yellow and (B) FA maps with parahippocampal gyrus outlined in yellow. C, Scatter plot of tau SUVr in the ERC/PRC versus parahippocampal gyral FA in amnestic and non-amnestic AD, MCI, and control subjects

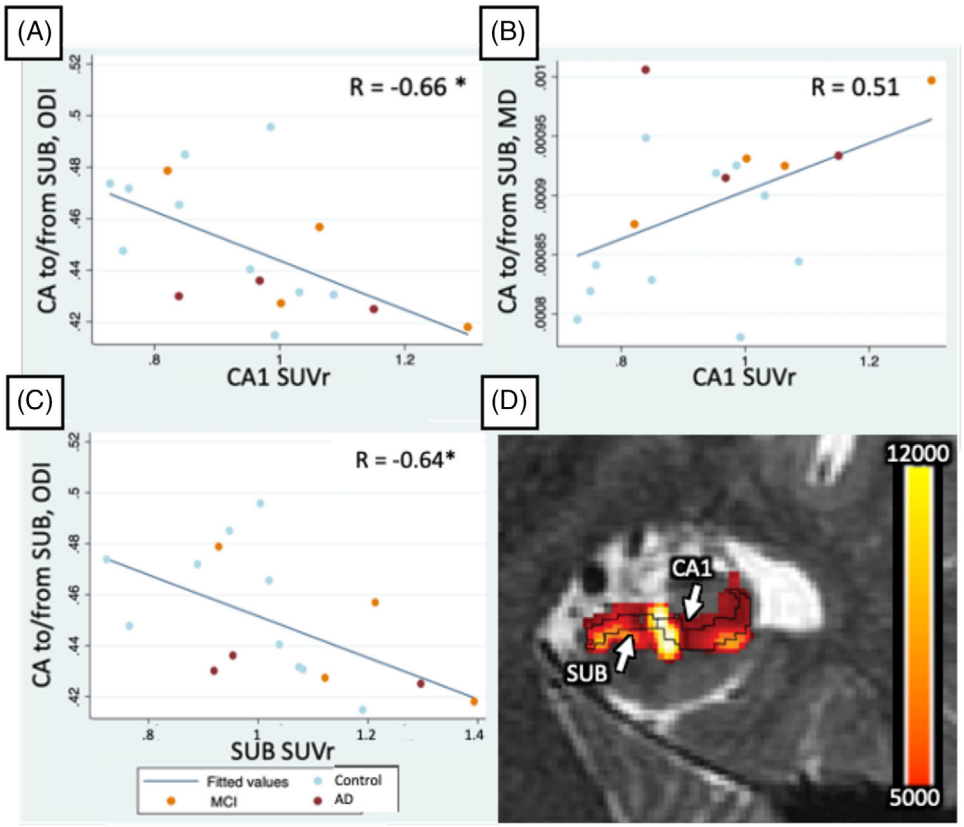

FIGURE 4 A-C, Significant ($P < .05$, or $P < .01$*) correlations between tau standardized uptake value ratio (SUVr) in subfields and cornu ammonis 1 (CA1)-to-subiculum tract-based diffusion metrics. R values are listed in the top right corner. D, CA1 to/from SUB streamline counts map interpolated and overlaid on the T2-weighted image

to-subiculum MD with CA1 SUVr ($P = .037$, R = 0.51; Figure 4B,D). In this same tract, ODI negatively correlated to both CA1 ($P < .01$, R = –0.66) and subiculum SUVr ($P < .01$, R = –0.64; Figure 4A,C).

There were no other significant differences in ROI or tractographic FA, MD, ODI, or FISO in other subfields, the fornix, or the whole hippocampus.

4 | DISCUSSION

In this study, we used simultaneous TOF PET and high-resolution MRI acquisition along with fine-tuned segmentations to analyze tau tracer accumulation and white matter connectivity in distinct hippocampal subfields. Our PET/MR image-based measurements correlated with known pathological progression of tau in the medial temporal lobe,[2] with the most significant involvement in ERC/PRC, and progressively less involvement further within the hippocampal formation. This finding parallels neuropathologic staging on a small scale that has not been previously demonstrated in vivo and could be useful in detecting subtle changes in tau accumulation during longitudinal studies in the future. ERC/PRC tau also correlated with PHG white matter integrity, as measured by FA, and was observable alongside hippocampal atrophy.

Our work expands upon existing tau-PET and MRI AD literature that has demonstrated correlations between tau deposition and AD status. ^{18}F-AV-1451 tau-PET binding patterns across larger regions of the brain, including the whole medial temporal lobe, correspond with known tau progression and Braak staging of disease.[36,37] Other studies using ^{18}F-AV-1451 have shown comparable results and spatial distributions of tracer uptake throughout the brain corresponding to amyloid status, cognition, and neuropathologic staging, beginning with heaviest involvement surrounding the transentorhinal area.[13,38]

Existing models of AD suggest that tau pathology, along with Aβ plaques, contribute to neuronal loss.[39] Our data support this, with ERC/PRC tau correlating with volume loss. Notably, the volume differences in DG, one of the last regions to accumulate tau within the hippocampus,[2,8] are not accompanied by significant tau tracer accumulation in AD/MCI in the same subregion, supporting the validity of the methods used in this study.

The tau tracer used, ^{18}F-PI-2620, is known to have lower off-target binding to Aβ and monoamine oxidase A and higher sensitivity and selectivity for pathologic tau aggregates than other tau tracers, including ^{18}F-AV-1451.[40] Previous work using different tau PET tracers has not found significant correlations between tau deposition and volume loss in hippocampal subfields;[41] however, this could be explained by differences in specific binding of tracers used, single-timepoint imaging, choroid plexus uptake, and limited resolution, but may still point toward the benefit of our method in evaluating hippocampal subfield-specific changes that may go undetected when evaluating the whole hippocampus.[42]

Subfield tau SUVr also correlated with diffusion MRI measurements. ERC/PRC tau was closely negatively correlated with ROI-based and tract-based PHG FA, and closely positively correlated to PHG tractographic ODI. Because the PHG is a region of crossing fibers, a weakening of the primary parahippocampal cingulum bundle would be expected to reduce the FA (with less uniform diffusion along the parahippocampal cingulum) and increase the ODI (with more relative dispersion).[43] This is consistent with FA alterations in parahippocampal white matter accompanying progression of AD.[15,44] We observed higher MD only between amnestic AD/MCI and controls, corroborating other work in which MD increases alongside memory decline.[45,46] These observations are consistent with work showing that tau accumulation contributes to axonal damage, which may also result in functional isolation of the hippocampus.[12] We also saw tract-based CA1 to SUB MD was higher in AD/MCI and accompanied by increased tau accumulation in both regions, suggesting that tau may mediate reductions in subregional cellularity. In the same tract, we found ODI is negatively correlated with tau uptake, which may be explained by there being a larger gray matter overlap of this smaller tract, with similar dendritic degradation reducing overall dispersion as measured by ODI.[43] Alternatively, given that this is in a region of extensive crossing fibers, much more so than the central parahippocampal gyrus in which the parahippocampal cingulum resides,[47] the decrease in ODI may simply reflect fewer overall crossing fibers (e.g., a weakening of the crossing perforant pathway).

To precisely correlate diffusion characteristics, volume loss, and tau deposition with disease severity in vivo, it is important to evaluate small subregions, which often requires long PET and MRI scan times. Thus, we used a TOF-PET/MR imaging acquisition method because it offers several benefits that help minimize image misregistration errors due to subject motion,[48] including that signal-to-noise ratio is increased compared to non-TOF images, and simultaneous acquisition enhances spatial alignment between PET and MRI image series.[49] Partial volume effects were minimized by doing a subfield erosion. Partial volume correction was not applied as research has shown that this does not significantly impact results.[50] Motion correction was not performed on this cohort, because our group had not, at the time of acquisition, developed an optical tracking technique to prospectively correct for motion in list mode PET; however, our motion correction approach will be used in future work.

Our results are limited by small sample size, so to increase statistical power we grouped AD and MCI for our analysis. Our future work will include analyses on larger cohorts. Nevertheless, the changes in volume and tau tracer accumulation, along with FA, are in the expected direction and magnitude given the patients' disease classification. Clinical implications may require a larger cohort and finer stratification based on cognitive ability. Other limitations of hippocampal subfield PET-MRI include fundamental resolution limitations of PET and only having approximate subfield segmentations at 3.0T MRI; in particular, CA2-4 is quite small and difficult to subdivide further. We hope to include more reliable hippocampal segmentation analyses using 7.0T MRI in the future, which would allow us to probe even smaller structural regions.

5 | CONCLUSION

We have used TOF-PET/MRI methods and a second-generation tau tracer to reveal subfield-level relationships between AD pathological hallmarks, connectivity, and volume effects patients, which has previously only been demonstrated using *post mortem* histology. Using these methods, we separated both amnestic and non-amnestic AD, MCI, and control subject groups. Our results indicate that tau accumulation and volumetric changes in the hippocampus are more pronounced than white matter degradation. Moreover, the effect size is larger in certain

AD hippocampal subfields compared to whole hippocampus, indicating that this type of analysis may enable earlier detection of tau pathology before it is apparent throughout the whole hippocampus. Combined with DTI, this approach reveals intricacies of subfield and subfield pathway degeneration intermingled with tau accumulation. Altogether, these results underline the potential value of subfield-specific imaging analyses using PET/MRI to track pathological hallmarks of AD in vivo. Quantifiable patterns of ^{18}F-PI2620 binding could be a valuable marker of AD progression or response to novel therapies in clinical trials, as well as help separate AD from other tauopathies.

CONFLICTS OF INTEREST

No potential conflicts of interest relevant to this article exist.

ACKNOWLEDGMENTS

This work was funded by the National Science Foundation Graduate Research Fellowship under grant no. DGE-1656518, NIA R01AG061120, R01 AG048076, K01 AG051718, R21 AG058859, American Society for Neuroradiology Boerger Research Fund for Alzheimer's Disease and Neurocognitive Disorders, Doris Duke Charitable Foundation, GE Healthcare, Stanford Wu Tsai Neuroscience Institute, and Stanford Precision Health and Integrated Diagnostics Center (PHIND). GZ declares royalties or licenses to him from Cambridge University Press and Stanford patents; he has also consulted for Biogen, received payment from AOCN and AOCNR, provided expert testimony to several legal firms, served on the board of trustees of ISMRM and Subtle Medical, which he cofounded. MC declares receiving a trainee award from ISMRM. GC declares receiving payment from MBCT at Stanford. MK declares patents on MR guided PET reconstruction methods. MJ declares serving on the board of directors of the World Molecular Imaging Society and Women in Molecular Imaging Network. EM declares receiving payments from Eli Lilly and Roche, and co-chairs the NIA ADRC Imaging Core steering committee.

REFERENCES

1. 2020 Alzheimer's disease facts and figures. Alzheimer's Dement., 16:391-460. https://doi.org/10.1002/alz.12068
2. Braak H, Alafuzoff I, Arzberger T, Kretzschmar H, Del Tredici K. Staging of Alzheimer disease-associated neurofibrillary pathology using paraffin sections and immunocytochemistry. *Acta Neuropathol*. 2006;112(4):389-404.
3. Strain JF, Smith RX, Beaumont H, et al. Loss of white matter integrity reflects tau accumulation in Alzheimer disease defined regions. *Neurology*. 2018;91(4):e313-e318.
4. Pereira JB, Ossenkoppele R, Palmqvist S, et al. Amyloid and tau accumulate across distinct spatial networks and are differentially associated with brain connectivity. Irish M, Behrens TE, eds. *Elife*. 2019;8:e50830.
5. Gendron TF, Petrucelli L. The role of tau in neurodegeneration. *Mol Neurodegener*. 2009;4(1):13.
6. Scelsi MA, Iglesias E, Schott JM, Ourselin S, Altmann A. The role of hippocampal subfields in the atrophy process in Alzheimer's disease: an in-Vivo study of the adni cohort. *Alzheimer's Dement*. 2017;13(7):P40-P41.
7. de Flores R, La Joie R, Landeau B, et al. Effects of age and Alzheimer's disease on hippocampal subfields: comparison between manual and freesurfer volumetry. *Hum Brain Mapp*. 2015;36(2):463-474.
8. Hett K, Ta VT, Catheline G, et al. Multimodal hippocampal subfield grading for Alzheimer's disease classification. *Sci Rep*. 2019;9(1):1-16.
9. West MJ, Coleman PD, Flood DG, Troncoso JC. Differences in the pattern of hippocampal neuronal loss in normal ageing and Alzheimer's disease. *Lancet*. 1994;344(8925):769-772.
10. Mueller SG, Schuff N, Yaffe K, Madison C, Miller B, Weiner MW. Hippocampal atrophy patterns in mild cognitive impairment and Alzheimer's disease. *Hum Brain Mapp*. 2010;31(9):1339-1347.
11. Vogels T, Leuzy A, Cicognola C, et al. Propagation of tau pathology: integrating insights from postmortem and in vivo studies. *Biol Psychiatry*. 2020;87(9):808-818.
12. Harrison TM, Maass A, Adams JN, Du R, Baker SL, Jagust WJ. Tau deposition is associated with functional isolation of the hippocampus in aging. *Nat Commun*. 2019;10(1):4900.
13. Maass A, Landau S, Baker SL, et al. Comparison of multiple tau-PET measures as biomarkers in aging and Alzheimer's disease. *Neuroimage*. 2017;157:448-463.
14. Carlson ML, DiGiacomo PS, Fan AP, et al. Simultaneous FDG-PET/MRI detects hippocampal subfield metabolic differences in AD/MCI. *Sci Rep*. 2020;10(1):12064.
15. La Rocca M, Amoroso N, Monaco A, Bellotti R, Tangaro S. A novel approach to brain connectivity reveals early structural changes in Alzheimer's disease. *Physiol Meas*. 2018;39(7):74005.
16. Fellgiebel A, Yakushev I. Diffusion tensor imaging of the hippocampus in MCI and early Alzheimer's disease. *J Alzheimer's Dis*. 2011;26(suppl 3):257-262.
17. Stebbins GT, Murphy CM. Diffusion tensor imaging in Alzheimer's disease and mild cognitive impairment. *Behav Neurol*. 2009;21:915041.
18. Berron D, van Westen D, Ossenkoppele R, Strandberg O, Hansson O. Medial temporal lobe connectivity and its associations with cognition in early Alzheimer's disease. *Brain*. 2020;143(4):1233-1248.
19. Mormino EC, Toueg TN, Azevedo C, et al. Tau PET imaging with 18F-PI-2620 in aging and neurodegenerative diseases. *Eur J Nucl Med Mol Imaging*. 2021;48(7):2233-2244.
20. Kroth H, Oden F, Molette J, et al. Discovery and preclinical characterization of [(18)F]PI-2620, a next-generation tau PET tracer for the assessment of tau pathology in Alzheimer's disease and other tauopathies. *Eur J Nucl Med Mol Imaging*. 2019;46(10):2178-2189.
21. Trelle AN, Carr VA, Wilson EN, et al. Association of CSF biomarkers with hippocampal-dependent memory in preclinical Alzheimer's disease. *Neurol Press*.
22. Sekine T, Buck A, Delso G, et al. Evaluation of atlas-based attenuation correction for integrated PET/MR in human brain: application of a head atlas and comparison to true CT-based attenuation correction. *J Nucl Med*. 2016;57(2):215-220.
23. Betthauser TJ, Cody KA, Zammit MD, et al. In vivo characterization and quantification of neurofibrillary tau PET radioligand (18)F-MK-6240 in humans from Alzheimer's disease dementia to young controls. *J Nucl Med*. 2019;60(1):93-99.
24. Modat M, Cash DM, Daga P, Winston GP, Duncan JS, Ourselin S. Global image registration using a symmetric block-matching approach. *J Med Imaging*. 2014;1(2):24003.
25. Parivash SN, Goubran M, Mills BD, et al. Longitudinal changes in hippocampal subfield volume associated with collegiate football. *J Neurotrauma*. 2019. (ja).
26. Yushkevich PA, Wang H, Pluta J, et al. Nearly automatic segmentation of hippocampal subfields in in vivo focal T2-weighted MRI. *Neuroimage*. 2010;53(4):1208-1224.
27. Csernansky JG, Wang L, Swank J, et al. Preclinical detection of Alzheimer's disease: hippocampal shape and volume predict dementia onset in the elderly. *Neuroimage*. 2005;25(3):783-792.
28. Yushkevich PA, Piven J, Hazlett HC, et al. User-guided 3D active contour segmentation of anatomical structures: significantly improved efficiency and reliability. *Neuroimage*. 2006;31(3):1116-1128.

29. Andersson JLR, Sotiropoulos SN. An integrated approach to correction for off-resonance effects and subject movement in diffusion MR imaging. *Neuroimage*. 2016;125:1063-1078.
30. Smith SM, Jenkinson M, Woolrich MW, et al. Advances in functional and structural MR image analysis and implementation as FSL. *Neuroimage*. 2004;23:S208-S219.
31. Jenkinson M, Beckmann CF, Behrens TEJ, Woolrich MW, Smith SM. FSL. *Neuroimage*. 2012;62(2):782-790.
32. Zhang H, Schneider T, Wheeler-Kingshott CA, DC Alexander. NODDI: practical in vivo neurite orientation dispersion and density imaging of the human brain. *Neuroimage*. 2012;61(4):1000-1016.
33. Behrens TEJ, Woolrich MW, Jenkinson M, et al. Characterization and propagation of uncertainty in diffusion-weighted MR imaging. *Magn Reson Med*. 2003;50(5):1077-1088.
34. Fischl B. FreeSurfer. *Neuroimage*. 2012;62(2):774-781.
35. Li J, Ji L. Adjusting multiple testing in multilocus analyses using the eigenvalues of a correlation matrix. *Heredity (Edinb)*. 2005;95(3):221-227.
36. Johnson KA, Schultz A, Betensky RA, et al. Tau positron emission tomographic imaging in aging and early Alzheimer's disease. *Ann Neurol*. 2016;79(1):110-119.
37. Ossenkoppele R, Schonhaut DR, Schöll M, et al. Tau PET patterns mirror clinical and neuroanatomical variability in Alzheimer's disease. *Brain*. 2016;139(5):1551-1567.
38. Schöll M, Lockhart SN, Schonhaut DR, et al. PET imaging of tau deposition in the aging human brain. *Neuron*. 2016;89(5):971-982.
39. Kametani F, Hasegawa M. Reconsideration of amyloid hypothesis and tau hypothesis in Alzheimer's disease. *Front Neurosci*. 2018;12:25.
40. Marquié M, Verwer EE, Meltzer AC, et al. Lessons learned about [F-18]-AV-1451 off-target binding from an autopsy-confirmed Parkinson's case. *Acta Neuropathol Commun*. 2017;5(1):75.
41. Sone D, Imabayashi E, Maikusa N, et al. Regional tau deposition and subregion atrophy of medial temporal structures in early Alzheimer's disease: a combined positron emission tomography/magnetic resonance imaging study. *Alzheimer's Dement (Amsterdam, Netherlands)*. 2017;9:35-40.
42. Okamura N, Harada R, Ishiki A, Kikuchi A, Nakamura T, Kudo Y. The development and validation of tau PET tracers: current status and future directions. *Clin Transl imaging*. 2018;6(4):305-316.
43. Colgan N, Siow B, O'Callaghan JM, et al. Application of neurite orientation dispersion and density imaging (NODDI) to a tau pathology model of Alzheimer's disease. *Neuroimage*. 2016;125:739-744.
44. Dalboni da Rocha JL, Bramati I, Coutinho G, Tovar Moll F, Sitaram R. Fractional anisotropy changes in parahippocampal cingulum due to Alzheimer's disease. *Sci Rep*. 2020;10(1):2660.
45. Shim G, Choi K-Y, Kim D, et al. Predicting neurocognitive function with hippocampal volumes and DTI metrics in patients with Alzheimer's dementia and mild cognitive impairment. *Brain Behav*. 2017;7(9):e00766.
46. Dalboni da Rocha JL, Bramati I, Coutinho G, Tovar Moll F, Sitaram R. Fractional anisotropy changes in parahippocampal cingulum due to Alzheimer's disease. *Sci Rep*. 2020;10(1):1-8.
47. Zeineh MM, Palomero-Gallagher N, Axer M, et al. Direct visualization and mapping of the spatial course of fiber tracts at microscopic resolution in the human hippocampus. *Cereb Cortex*. 2016;27(3):1779-1794.
48. Metere R, Kober T, Möller HE, Schäfer A. Simultaneous quantitative MRI mapping of T1, T2* and magnetic susceptibility with multi-echo MP2RAGE. *PLoS One*. 2017;12(1):e0169265.
49. Monti S, Cavaliere C, Covello M, Nicolai E, Salvatore M, Aiello M. An evaluation of the benefits of simultaneous acquisition on PET/MR coregistration in head/neck imaging. *J Healthc Eng*. 2017;2017:2634389.
50. Vogel JW, Iturria-Medina Y, Strandberg OT, et al. Spread of pathological tau proteins through communicating neurons in human Alzheimer's disease. *Nat Commun*. 2020;11(1):2612.

SUPPORTING INFORMATION

Additional supporting information may be found online in the Supporting Information section at the end of the article.

How to cite this article: Carlson ML, Toueg TN, Khalighi MM, et al. Hippocampal subfield imaging and fractional anisotropy show parallel changes in Alzheimer's disease tau progression using simultaneous tau-PET/MRI at 3T. *Alzheimer's Dement*. 2021;13:e12218. https://doi.org/10.1002/dad2.12218